Numerical simulation of the effects of a solar energetic particle event on the ionosphere of Mars

Varun Sheel,[1] S. A. Haider,[1] Paul Withers,[2] K. Kozarev,[2] I. Jun,[3] S. Kang,[3] G. Gronoff,[4] and C. Simon Wedlund[5]

Received 15 December 2011; revised 22 February 2012; accepted 1 April 2012; published 12 May 2012.

[1] We investigate the ionospheric effects of a solar energetic particle (SEP) event at Mars, specifically the 29 September 1989 event. We use its energy spectrum and a steady state ionospheric model to simulate vertical profiles of ion and electron densities. The ionospheric response to this large event would have been readily observable. It caused electron densities to exceed 10^4 cm^{-3} at 30–170 km, much larger than typically observed below 100 km. It also increased the ionosphere's total electron content by half of its subsolar value and would have caused strong attenuation of radio waves. The simulated attenuation is 462 dB at 5 MHz, which demonstrates that SEP events can cause sufficient attenuation (>13 dB) to explain the lack of surface reflections in some MARSIS topside radar sounder observations. We also develop a complementary generalized approach to the study of the ionospheric effects of SEP events. This approach predicts the threshold intensities at which a SEP event is likely to produce detectable changes in electron density profiles and radio wave attenuation measurements. An event one hundred times less intense than the 29 September 1989 event produces electron densities in excess of 3000 cm^{-3} at 80 km, which should be measurable by radio occultation observations, and causes sufficient attenuation to eliminate MARSIS surface reflections. However, although enhancements in total electron content have been observed during SEP events, predicted enhancements in low altitude electron density were not confirmed by observations.

Citation: Sheel, V., S. A. Haider, P. Withers, K. Kozarev, I. Jun, S. Kang, G. Gronoff, and C. Simon Wedlund (2012), Numerical simulation of the effects of a solar energetic particle event on the ionosphere of Mars, *J. Geophys. Res.*, *117*, A05312, doi:10.1029/2011JA017455.

1. Introduction

[2] Solar energetic particle (SEP) events are major disturbances in the heliosphere [*Schrijver and Siscoe*, 2010]. Energetic particle densities in the solar wind are significantly enhanced during SEP events, which can have substantial impacts on the magnetospheres, ionospheres, and neutral atmospheres of any planets they encounter. Observations by the MARSIS topside radar sounder have demonstrated that SEP events modify the ionosphere of Mars [*Morgan et al.*, 2006]. The instrument does not detect its usual reflections from the surface of Mars during an SEP event, indicating that radio waves that usually pass smoothly through the ionosphere are instead absorbed. Radio waves transmitted by the MARSIS topside radar sounder are affected by radio wave absorption in the ionosphere. Electrons accelerated by the passing radio wave dissipate energy if they collide with neutral particles [*Budden*, 1985; *Withers*, 2011], and if the attenuation is severe, then no return signals are received by MARSIS. Severe attenuation implies higher-than-usual electron densities in regions with sufficient neutral densities for absorption to occur. In particular, the lack of surface reflections in MARSIS observations at 5 MHz indicate a one-way power loss of 13 dB or more [*Nielsen et al.*, 2007]. However, no previous work has shown that the electron density profile is sufficiently enhanced during an SEP event for the ionospheric attenuation to reach the required threshold [*Withers*, 2011]. Therefore our aim in this work is to simulate the vertical structure of the ionosphere of Mars during a large SEP event and test whether the resultant ionospheric modifications are sufficient to cause MARSIS blackouts [*Withers*, 2009]. This aim is also motivated by basic scientific interest in how the ionosphere is modified by an SEP event and whether these changes are readily detectable [*Leblanc et al.*, 2002; *Parkinson et al.*, 2010]. We adopt straight-forward methods in order to minimize the sensitivity

[1]Physical Research Laboratory, Ahmedabad, India.
[2]Astronomy Department, Boston University, Boston, Massachusetts, USA.
[3]Jet Propulsion Laboratory, California Institute of Technology, Pasadena, California, USA.
[4]NASA Langley Research Center, Hampton, Virginia, USA.
[5]Belgian Institute for Space Aeronomy, Brussels, Belgium.

Corresponding author: Paul Withers, Astronomy Department, Boston University, 725 Commonwealth Ave., Boston, MA 02215, USA. (withers@bu.edu)

0148-0227/12/2011JA017455

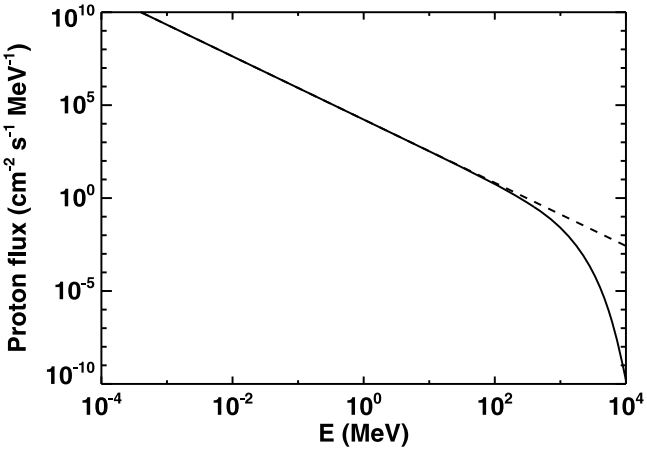

Figure 1. Proton energy spectrum during 29 September 1989 SEP event (solid line). The dashed line shows an analytical approximation to the spectrum, $2\pi k\left(E/E_{ref}\right)^{-\gamma}$, which is introduced in section 4.

of our results to the uncertain atmospheric environment at Mars and the uncertain energetic particle flux at Mars. This approach illustrates the key physical processes as clearly as possible and can readily be applied to broad-based follow-on work, as opposed to carefully crafted case studies in which every aspect is optimized for one specific event — and the results cannot be generalized beyond that narrow focus.

[3] Section 2 reports a focused simulation of ionospheric plasma densities during the large SEP event of 29 September 1989. Section 3 discusses the observable consequences of the predictions of section 2. Section 4 develops and evaluates a generalized simulation approach that complements the approach of section 2. Section 5 presents the conclusions of this work.

2. Focused Simulation of Predicted Ionospheric Densities During an SEP Event

[4] Consideration of the basic physics of how energetic particles interact with a fluid atmosphere inevitably leads to the conclusion that some of the energy deposited into the atmosphere by the decelerating particles ionizes atmospheric species and therefore enhances plasma densities above their quiescent values. This process is well-known in the terrestrial environment as the cause of polar cap absorption events [*Bailey*, 1964; *Patterson et al.*, 2001]. These are events in which radio waves passing through the polar atmosphere are attenuated much more strongly than usual as a result of increased plasma densities at the relatively low altitudes where electron-neutral collisions are efficient at draining energy from the radio wave [*Budden*, 1985]. For Earth, the strong geomagnetic field focuses incident energetic particles towards the polar caps. Similar behavior is expected at Mars, except that the lack of a strong core dynamo means that such radio wave absorption will not be limited to the poles. We are not aware of any previous simulations of ionospheric plasma densities on Mars during an SEP event, although *Leblanc et al.* [2002] simulated the vertical profile of energy deposition rate for an SEP event, using a set of approximations for the description of the energy transport of high-energy ions in the Martian atmosphere. In this section, we describe how we used an SEP spectrum to predict the vertical profile of energy deposition in the atmosphere, converted this into a vertical profile of ionization rate, and used an ionospheric model to predict vertical profiles of ion and electron densities. Analysis of the predicted ionospheric properties follows in section 3. We label the results of this section as those of the "focused simulation".

2.1. Energy Spectrum

[5] The energy spectrum of an SEP event has a significant impact on how the energy of SEPs is dissipated in the atmosphere. The highest energy particles will barely be decelerated by the atmospheric column at all, transferring their energy to the surface upon impact. Moderate energy particles will be decelerated to thermal speeds after descending partway through the atmospheric column, transferring their energy into ionization events across that range of altitudes. The lowest energy particles will be decelerated at very high altitudes in the atmosphere and thus will not contribute to ionization at lower altitudes.

[6] All SEP events are different, which makes the selection of an SEP spectrum for analysis a major decision. Since an aim in this paper is to test the basic viability of the hypothesis that SEP events can cause MARSIS blackouts, we chose a particularly large SEP event from 29 September 1989. The proton energy spectrum of the SEP event of 29 September 1989 was reported by *Lovell et al.* [1998] using IMP and GOES data. Although solar wind plasma contains a range of species that should be included in comprehensive studies, protons are the dominant species [e.g., *Reames et al.*, 2001]. Therefore we ignored species other than protons in the exploratory work. *Lovell et al.* [1998] found that dJ/dE, the proton flux at Earth, satisfied:

$$\frac{dJ}{dE} = k(E/E_{ref})^{-\gamma}\exp(-E/E_0) \tag{1}$$

where E is energy in the range 1–10^4 MeV, k = 6000 cm^{-2} s^{-1} sr^{-1} MeV^{-1}, γ = 1.7, E_{ref} = 1 MeV, and E_0 = 600 MeV. The results of *Lovell et al.* [1998] are limited to energies of 1 MeV and above, which is not sufficient for this work. Since lower energy protons play an appreciable role at altitudes above 100 km (section 2.2), we assumed that equation (1) was valid down to energies of 10^{-4} MeV or 0.1 keV. This assumption is reasonable above 0.01 MeV, but underestimates the true flux at lower energies where fast solar wind protons are abundant [*Jokipii et al.*, 1997; *Leblanc et al.*, 2002; *Meyer-Vernet*, 2007]. As subsequent sections show, the findings of this work arise from the effects of protons with energies in excess of 0.01 MeV, so our extension of the energy spectrum to 0.1 keV is primarily a convenience to ensure smoothness. Correcting to the heliocentric distance of Mars (1.5 AU) reduces k from 6000 cm^{-2} s^{-1} sr^{-1} MeV^{-1} by a factor of 1.5^2. The solid angle dependence in dJ/dE was removed by multiplying by 2π sr [e.g., *Haider et al.*, 2009] to obtain the proton flux per unit area per unit time per unit energy. This flux, which is shown in Figure 1, has an integrated energy flux incident on the top of the Martian atmosphere of 3.3×10^5 MeV cm^{-2} s^{-1}.

2.2. Energy Deposition

[7] Energetic protons are decelerated by interactions with neutral molecules as they descend into the Martian atmosphere. The interaction of neutrals and charged particles, where the consequences may encompass charge exchange, scattering, and the fates of electrons stripped from neutrals, involves many complicated processes. The most critical aspect for simulating the ionospheric effects of an SEP event is the vertical profile of energy deposition in the atmosphere. We elected to use a straight-forward and easily reproducible method to determine this vertical profile, namely the continuous slowing down approximation. This has extensive heritage for first studies of the interaction of energetic particles and neutrals in a planetary atmosphere [*Rees and Jones*, 1973; *Porter and Green*, 1975; *Galand et al.*, 1997; *Kallio and Barabash*, 2001; *Agren et al.*, 2007; *Fox et al.*, 2008, and references therein]. This approach involves two key assumptions. First, that every proton of energy E travels the same distance (range) R before coming to rest (or, more accurately, being thermalized) at their stopping altitude. Secondly, that the deposition of energy by protons of initial energy E between the top of the atmosphere and their stopping altitude is proportional to the local atmospheric density. We obtained values of R, specifically the projected range, for carbon dioxide as a function of E (10^{-3}–10^{4} MeV) from the Physical Measurement Laboratory of the National Institute of Standards and Technology [*Berger et al.*, 2005], then extrapolated to reach 10^{-4} MeV. The energy-dependent range is shown in Figure 2a in units of mass per unit area, or column density. The altitude at which a proton of a specified initial energy comes to rest (stopping altitude) was calculated using these ranges and the atmospheric model, and is shown in Figure 2b. For instance, protons with an initial energy of 7 MeV come to rest at 60 km. Note that, since protons with initial energies of 10^{-4}, 0.01, and 1 MeV are stopped at 200, 150, and 100 km respectively (Figure 2b), our extrapolation of the energy spectrum below 0.01 MeV is irrelevant for results below 150 km. Protons of a particular initial energy deposit all their energy at altitudes above their stopping altitude and none at lower altitudes. The second assumption leads to the following expression for $Q(E, z)\,dzdE$, the energy deposited between altitudes z and $z + dz$ per unit area per unit time from protons with initial energy in the range E to $E + dE$:

$$Q(E,z)\,dzdE = 2\pi\frac{dJ}{dE}E\frac{\rho(z)dz}{R(E)}dE \text{ if } \int_{z'=z}^{z'=\infty}\rho(z')dz' < R$$
$$Q(E,z)\,dzdE = 0 \text{ if } \int_{z'=z}^{z'=\infty}\rho(z')dz' > R \quad (2)$$

[8] An energy deposition rate, shown in Figure 2c as a function of altitude and energy, was calculated using vertically incident protons and carbon dioxide abundances from

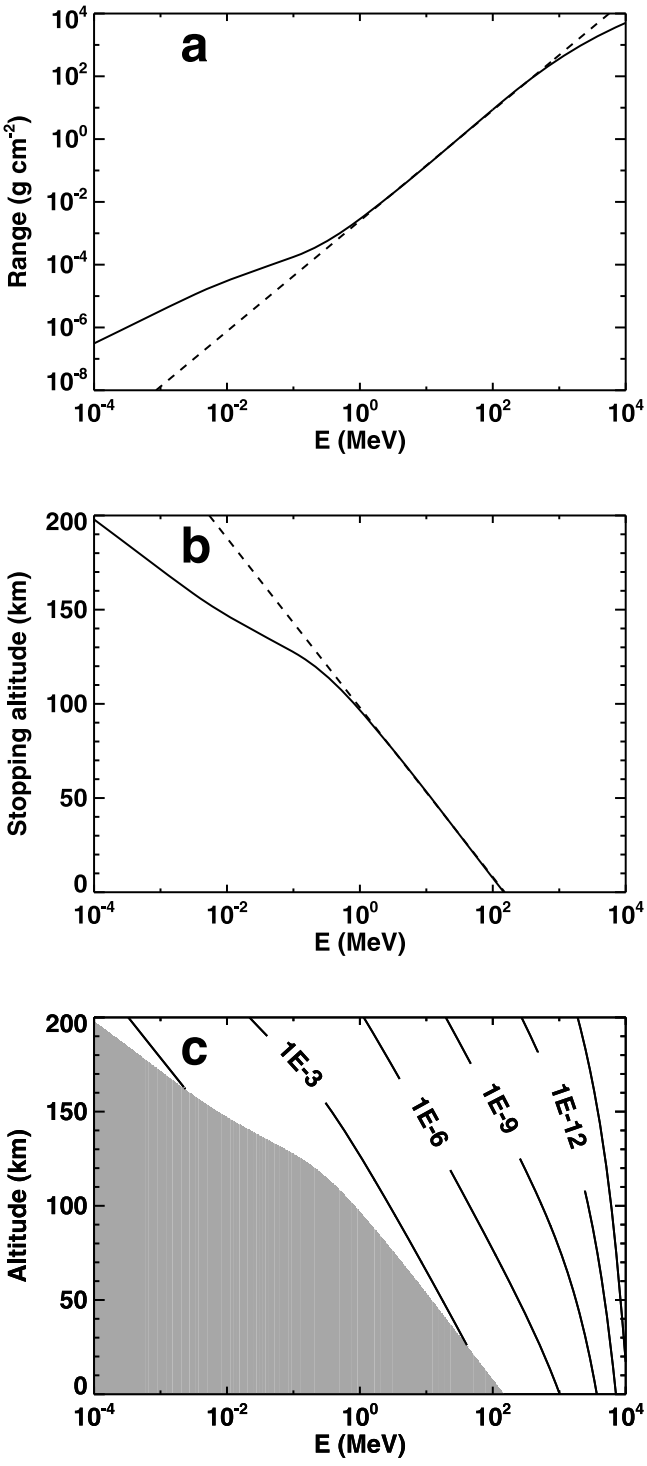

Figure 2. (a) Range of protons in CO_2 as function of energy (solid line). Range is expressed as a column density in units of g cm^{-2}. The dashed line shows a fit to the range for energies 1–500 MeV, which is introduced in section 4. (b) Altitude at which vertically incident protons have descended through a Martian atmospheric column density equal to their range as a function of initial energy. Protons with initial energies greater than 100 MeV are not stopped by the atmosphere. The dashed line shows an analytical approximation to the stopping altitude, which is introduced in section 4. (c) $Q(E, z)$, the energy deposition rate, as a function of energy and altitude for the continuous slowing down approximation approach to energy deposition. The units of $Q(E, z)$ are MeV cm^{-3} s^{-1} MeV^{-1} or cm^{-3} s^{-1}. No energy deposition occurs in the shaded area, which corresponds to altitudes below the stopping altitude of a particular proton energy.

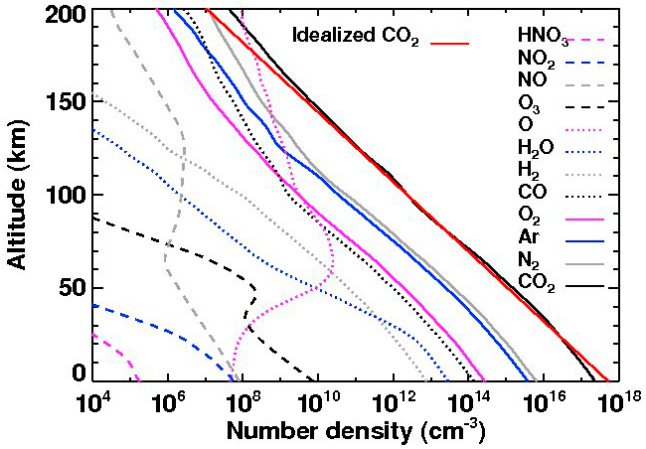

Figure 3. Neutral atmospheric model of *Haider et al.* [2009], which is used in the focused simulation. The red line shows the idealized atmosphere introduced in section 4, which is used in the generalized simulations.

the neutral atmospheric model of *Haider et al.* [2009] (0–200 km), shown in Figure 3. Inclusion of other species, which total less than 5% of the total number density, will have a negligible effect on the conclusions of this manuscript. The energy-integrated vertical profile of energy deposition rate is shown in Figure 4a. Figure 2 shows that most energy deposited at a given altitude is deposited by protons that have almost reached their limiting range. For instance, 50% of the energy deposition rate at 70 km derives from protons with initial energies of less than 7 MeV — and only protons with initial energies greater than 4 MeV reach 70 km.

[9] Protons with initial energies of 10^{-4}, 0.01, and 1 MeV are stopped at 200, 150, and 100 km respectively (Figure 2b). Thus our extrapolation of the energy spectrum below 0.01 MeV is irrelevant for results below 150 km.

[10] More sophisticated models of the interactions of protons and neutral species exist that could be applied to this problem. For energies lower than typically 100 keV, relativistic effects (for instance bremsstrahlung and Cherenkov effect) and spallation processes [e.g., *Deghfel et al.*, 2009] may be neglected. At these energies, the transport of protons can be described as a coupled H^+/H system of kinetic Boltzmann equations, requiring the inclusion of charge-exchange reactions, ionization and excitation mechanisms [e.g., *Basu et al.*, 1993; *Bisikalo et al.*, 1996; *Galand and Chakrabarti*, 2002; *Fox et al.*, 2008]. In only a few studies because of its complexity, angular redistribution due to collisions and magnetic effects have been calculated, using the continuous slowing down approximation (valid in the energy range considered) to simplify the equations [*Galand et al.*, 1997; *Simon et al.*, 2007]. In this respect, adaptation to the atmosphere of Mars demands an immense investment of time outside the scope of the present general study. For higher energies, nuclear processes cannot be neglected, and the whole electromagnetic cascade must be computed [*Gaisser*, 1990]. To account for these processes, several cosmic ray precipitation models have been developed and adapted to planetary studies including but not restricted to Earth, Mars or Titan [e.g., *O'Brien*, 1969; *Capone et al.*, 1976; *Mertens et al.*, 2010]. The Planetocosmics model is one such model adapted to several planetary atmospheres including Mars and is based on the GEANT4 Monte-Carlo library [*Desorgher et al.*, 2005]. This code has recently been coupled with the Aeroplanets-Trans* kinetic model to account for the transport of secondary electrons produced in the electromagnetic cascade [*Gronoff et al.*, 2009, 2011].

[11] The current focus of our work does not merit such complexity. Nevertheless, we did conduct simulations using the Planetocosmics model adapted to the present SEP study of the Martian atmosphere. This model predicted energy deposition rates that were somewhat smaller than those shown in Figure 4, with the discrepancy being most pronounced at low altitudes. A likely cause of this difference is that the continuous slowing down approximation, although excellent below 100 keV, becomes progressively weaker at higher energies, and higher energies dominate the energy deposition at lower altitudes. Thus the plasma densities that we derive in subsequent sections using the results of the continuous slowing down approximation will be upper bounds. However, the Planetocosmics model suggests that these plasma densities are over-estimated by no more than a factor of three. As will be shown, that level of accuracy is sufficient for the purposes of this work, especially if

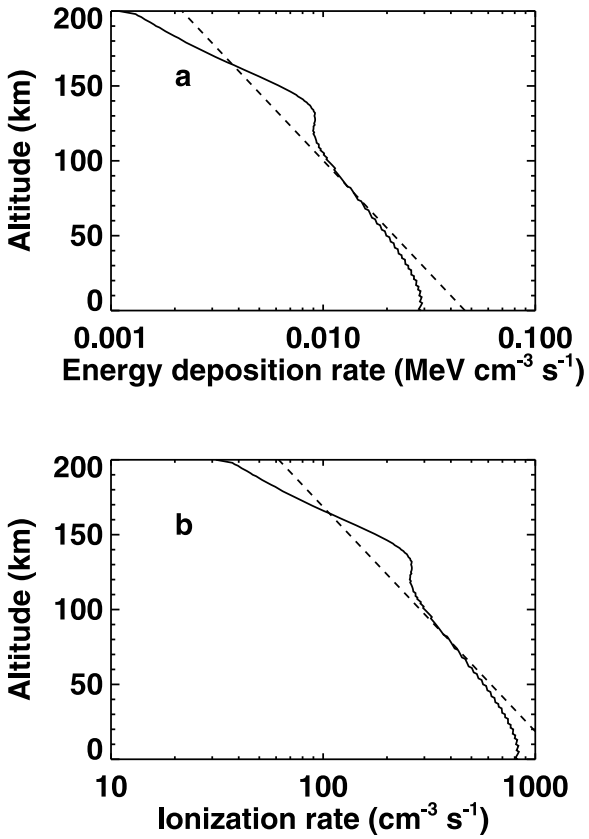

Figure 4. (a) Energy deposition rate profile calculated using the continuous slowing down approximation (black solid line, section 2.2) approach to energy deposition. The dashed line shows an analytical approximation to the energy deposition rate, which is introduced in section 4. (b) Same as Figure 4a but showing the ionization rate calculated as the ratio of the energy deposition rate to 35 eV.

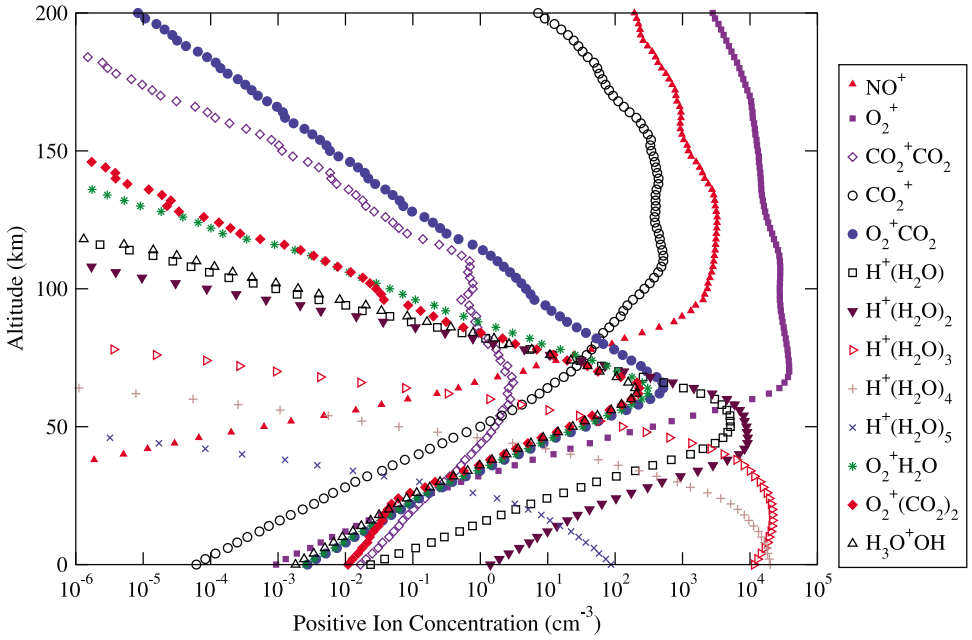

Figure 5. Positive ion densities predicted by focused simulation of 29 September 1989 SEP event, neglecting photoionization by solar irradiance. Thus ion densities are unrealistically low above 100 km.

the lack of observational constraints on knowledge of SEP spectra at Mars with good spectral and temporal resolution, of the relevant ionospheric reaction rate constants and of the neutral atmosphere composition are considered.

2.3. Ionospheric Densities

[12] We estimated a total ionization rate, I_{total}, which is shown in Figure 4b, from the energy deposition rate profile by assuming that each 35 eV of deposited energy creates one ion-electron pair [e.g., *Rees and Jones*, 1973; *International Commission on Radiation Units and Measurements*, 1993; *Haider et al.*, 2009]. The ionospheric model of *Haider et al.* [2009] was used to determine steady state ion densities from this ionization rate. Use of a pure carbon dioxide atmosphere at this point would have generated highly erroneous ion densities due to the important role of trace species in ionospheric chemistry, so all neutral species in the model of *Haider et al.* [2009] were included. The total ionization rate from Figure 4b was generalized to all species by assuming that the ionization rate of neutral species j, I_j,

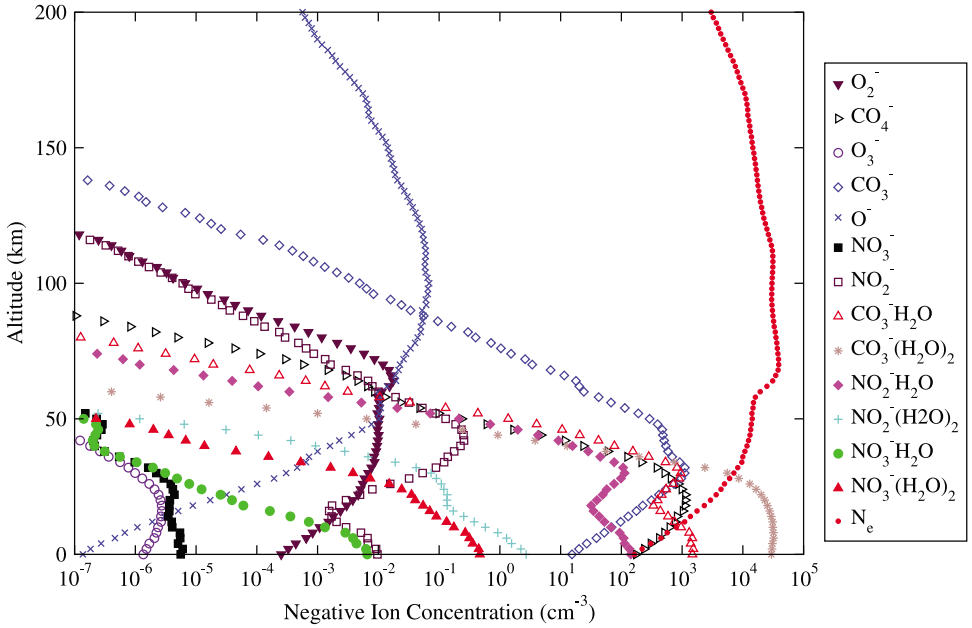

Figure 6. Negative ion densities predicted by focused simulation of 29 September 1989 SEP event, neglecting photoionization by solar irradiance. Thus ion densities are unrealistically low above 100 km.

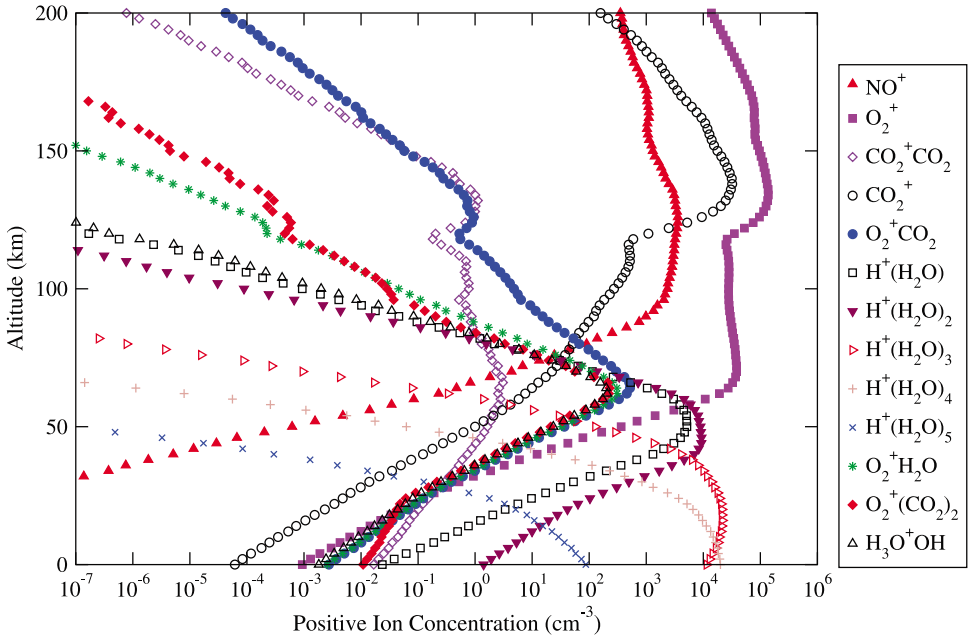

Figure 7. Positive ion densities predicted by focused simulation of 29 September 1989 SEP event, including subsolar photoionization by solar irradiance.

satisfies $I_j/I_{total} = n_j/n_{total}$, where n is neutral number density. The steady state assumption merits some justification. The energy spectrum derived by *Lovell et al.* [1998], although representing the peak of the SEP event, is based on hourly averages of particle data. Thus our input SEP flux can be accepted as persisting for one hour. Furthermore, *Lario et al.* [2009] show that the SEP flux in this and many other SEP events decays from its peak value over a timescale of about a day. Molecular ion lifetimes are generally on the order of minutes, not hours, for densities greater than 10^4 cm^{-3} [*Schunk and Nagy*, 2000; *Martinis et al.*, 2003; *Fox and Yeager*, 2006].

[13] Two separate ionospheric simulations are reported in Figures 5, 6, 7, and 8. One uses only the SEP energy deposition as an ionization source. The other augments this with solar photoionization, q, which we represent by:

$$q = q_0 \exp\left(1 - x - \exp\left(-x\right)\right) \tag{3}$$

where q_0, the peak photoionization rate, is 10^4 cm^{-3} s^{-1} and x is $(z - z_0)/H$, where z is altitude, z_0 is the altitude of peak photoionization (120 km), and H is the neutral scale height [*Withers*, 2009]. This simple Chapman approximation is sufficient for the purposes of this work. The simulated electron density profiles are shown more clearly in Figure 9.

[14] The electron densities produced by the SEP-only simulation exceed 10^4 cm^{-3} between 30 km and 170 km. In both simulations, electron densities during the SEP event are predicted to be much larger than usual between 30 km and 100 km.

2.4. Comparison to Ionospheric Effects of Galactic Cosmic Rays

[15] The simulated profiles of ionization rates and ion densities reported here for a large SEP event, which occurs infrequently, can be compared to similar simulations for the steady background flux of galactic cosmic rays reported by *Haider et al.* [2009]. The results of *Haider et al.* [2009] are dominated by photoionization, not ionization from galactic cosmic rays, above 100 km. Below 100 km, their ionization rate is proportional to neutral number density, which is as expected for an incident particle flux in which no significant subset of particles has yet reached their stopping altitude. This occurs because the galactic cosmic ray spectrum is dominated by particles with energies in excess of 100 MeV, which are not stopped by the atmosphere before they reach the ground (Figure 2b). The energy flux associated with galactic cosmic rays is smaller than for SEP events, but typical galactic cosmic rays have greater energies than typical solar energetic particles. The ionization rates found for this focused simulation of a large SEP event are three orders of magnitude greater than those of *Haider et al.* [2009] at the surface, and this ratio increases with increasing altitude up to 100 km, where the results of *Haider et al.* [2009] become dominated by photoionization, not ionization from galactic cosmic rays. The ion chemistry is similar between this work and *Haider et al.* [2009]. O_2^+ is the dominant positive species above 60–70 km altitude with water group cations dominant at lower altitudes, while electrons remain the dominant negative species until replaced below about 20 km by $CO_3^-(H_2O)_2$. Yet the ion densities are vastly different. Even in the case with only the SEP energy deposition as an ionization source (Figures 5 and 6), this work predicts electron densities in excess of 10^4 cm^{-3} from 30 km to 170 km. Electron densities in *Haider et al.* [2009] are less than 10^2 cm^{-3} below 75 km and their increase to 10^4 cm^{-3} at 100 km is mainly driven by photoionization, rather than being solely caused by energetic particles. The ionospheric effects of rare SEP events greatly exceed the effects of incessant galactic cosmic rays.

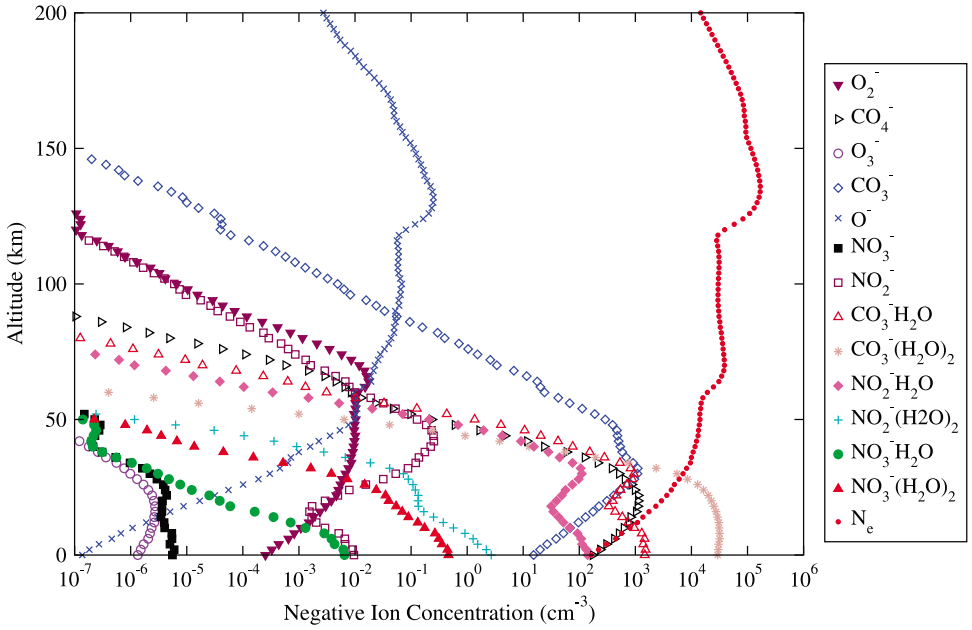

Figure 8. Negative ion densities predicted by focused simulation of 29 September 1989 SEP event, including subsolar photoionization by solar irradiance.

2.5. Comparison to Previous Work

[16] Ongoing research in this area was reported recently by *Parkinson et al.* [2010] and related studies have been described by *Luhmann and Kozyra* [1991] and *Kallio and Barabash* [2001]. However the most comparable published work is that of *Leblanc et al.* [2002], who have also simulated the vertical profile of energy deposition rate for an SEP event by means of a combination of separate 3D Monte Carlo and analytical ion stopping and range models from the magnetosphere to ionospheric altitudes, although they did not explore the ionospheric consequences. They focused on the 20 October 1995 event and their simulated profile of energy deposition rate is reproduced in Figure 10. It can be compared to the profile of energy deposition rate found for the 29 September 1989 event by this work's focused simulation (Figure 4a). The event studied by *Leblanc et al.* [2002] had a flux at Earth of 10^3 protons cm^{-2} s^{-1} sr^{-1} MeV^{-1} at energies of 1 MeV, about three times smaller than the value

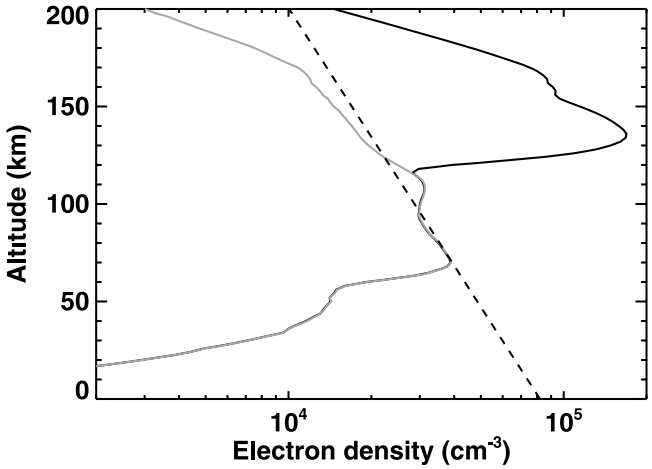

Figure 9. Electron density profile predicted by focused simulation of the 29 September 1989 SEP event, neglecting photoionization (grey solid line) and including subsolar photoionization (black solid line). These two profiles are identical below 100 km. The black dashed line shows the electron density profile from the generalized model of section 4.

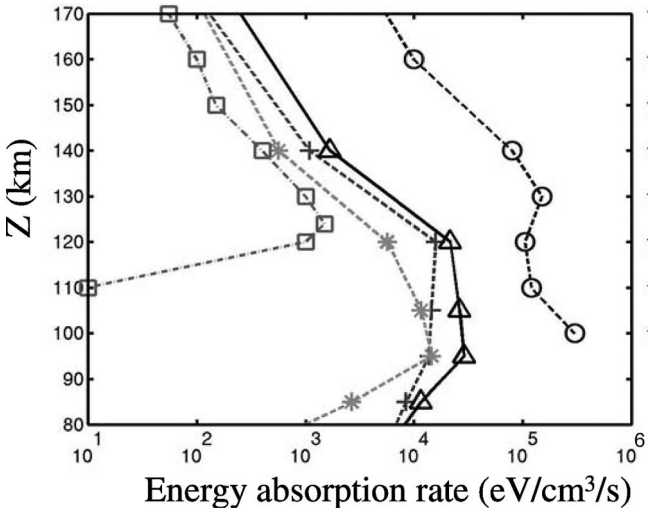

Figure 10. Profile of energy deposition rate reported by *Leblanc et al.* [2002] for 20 October 1995 SEP event. Crosses (show) energy deposition due to SEP H particles. Triangles show total energy deposition due to SEP H and He. Squares show energy deposition due to energetic neutral atoms as calculated by *Kallio and Barabash* [2001]. Circles show energy deposition due to EUV/UV flux [*Fox and Dalgarno*, 1979].

of 2667 protons cm^{-2} s^{-1} sr^{-1} MeV^{-1} adopted in section 2.1. The simulated energy deposition rates at 90 km are very similar, slightly in excess of 10^{-2} MeV cm^{-3} s^{-1}. The results of *Leblanc et al.* [2002] show energy deposition rates decreasing with decreasing altitude below 90 km, in contrast to our results, and smaller values around 150 km than in our results. *Leblanc et al.* [2002] used a power law exponent of −2.4 in contrast to our exponent of −1.7, which is likely to account for some of these differences. Other likely explanations include differences in our neutral atmospheres and representations of proton deceleration.

3. Observable Consequences of Predictions

[17] In this section, we explore several ways in which the predictions of the preceding sections can be tested. We consider radio occultation observations, and orbiting radar measurements of total electron content and ionospheric attenuation.

3.1. Radio Occultation Observations

[18] An observation by current or past radio occultation experiments of an electron density profile like Figure 9 would be distinctly different from typical observations made outside the influence of an SEP event [e.g., *Withers*, 2009]. The primary differences would be atypically large electron densities below 100 km that extend for tens of kilometers. Although atypically large electron densities below 100 km can also be caused by other sporadic events, such as solar flares or meteoroid ablation, these produce narrower plasma layers than predicted in Figure 9 [*Mendillo et al.*, 2006; *Withers et al.*, 2008]. We conducted a search for such enhancements in electron density using ionospheric electron density profiles from the Mars Global Surveyor (MGS) radio occultation instrument [*Hinson et al.*, 1999; *Withers et al.*, 2008], concentrating on intervals when an increase in the background signal of the MGS Electron Reflectometer (ER) indicated the occurrence of an SEP event at Mars [*Lillis et al.*, 2010]. These intervals were identified based on MGS ER information provided by D. Brain. Electron densities measured at 95 km before, during, and after an SEP event were compared, yet no striking instances of elevated densities during SEP events were discovered.

3.2. Orbiting Radar Measurements of Total Electron Content

[19] Orbiting radar experiments, although not able to measure vertical electron density profiles with the necessary vertical range, can make indirect measurements of the ionospheric effects of an SEP event. The subsurface mode of the MARSIS topside radar sounder on Mars Express measures the column density of ionospheric electrons, or total electron content (TEC) [*Lillis et al.*, 2010]. The TEC of the electron density profile produced by our focused simulation of the ionization caused by solar energetic particles only (neglecting photoionization) is 3.5×10^{11} cm^2, about half of the subsolar TEC of 8×10^{11} cm^2 [*Mendillo et al.*, 2004]. It is equivalent to the ionospheric TEC at a solar zenith angle of 70 degrees [*Withers*, 2009]. A significant increase in TEC across a wide geographic area at a time when particles and fields instruments at Mars detect an SEP event would be a robust detection of the ionospheric response to the SEP event.

[20] *Lillis et al.* [2010] reported increases in TEC during two SEP events at Mars in July 2005 and December 2006. Dayside total electron content increased from its background value by about 100%–200% during the July 2005 event and 20%–50% during the December 2006 event. These SEP events were characterized by their effects on the background signal of two instruments at Mars, the MGS Electron Reflectometer (ER) and the Mars Express (MEX) Analyzer of Space Plasmas and Energetic Atoms (ASPERA) Electron Spectrometer (ELS), rather than using a directly measured SEP spectrum. The peak increase in the ASPERA ELS SEP proxy was greater in December 2006 than in July 2005, yet the increase in TEC was greater for the July 2005event than the December 2006 event, which is a conundrum. This may be explained by the fact that the July 2005 period was characterized by several long-lived SEP events, whereas the December 2006 period was characterized by a single brief SEP event. In future work, we plan to simulate the SEP spectrum at Mars during these events and quantitatively test the predictions of this work.

3.3. Orbiting Radar Measurements of Radio Wave Absorption by the Ionosphere

[21] Do the enhanced electron density profiles shown in Figure 9 cause sufficient radio wave absorption to explain the observed lack of MARSIS surface reflections during SEP events? This requires 13 dB of attenuation at 5 MHz [*Nielsen et al.*, 2007]. We used the principles outlined in *Withers* [2011, section 2.2] to calculate the frequency-dependent attenuation that would be caused by the electron density profiles in Figure 9. As in *Withers* [2011], we took the electron-neutral collision frequency to be the product of the neutral number density and a constant, 10^{-13} m^3 s^{-1}. The resultant power loss is shown in Figure 11. The attenuation at 5 MHz, 462 dB for the SEP-only simulation, easily exceeds the 13 dB required to disrupt MARSIS observations. If our predicted attenuation, derived using the energy spectrum from the peak of a particularly large SEP event, did not greatly exceed 13 dB, then we would have to question either whether our predicted ionospheric densities are correct or whether the basic concept of MARSIS disruption by enhanced plasma densities caused by the impact ionization of energetic particles in an SEP event is correct.

[22] Appreciable attenuation persists to remarkably high frequencies, exceeding 1 dB up to about 0.5 GHz and 0.1 dB up to about 2 GHz. Orbiter-lander communications on Mars use 400 MHz frequencies and Earth-lander communications use ∼5 GHz [*Withers*, 2011]. Correlations between observed diminution of signal strength below nominal values and the energetic particle environment at Mars may provide another data set for studying the ionospheric response to SEP events. Particularly valuable characteristics of this additional data set would be its long duration (MARSIS only operates for brief intervals around periapsis) and actual attenuation measurements (in contrast to the binary "exceeds/does not exceed 13 dB" observation of MARSIS).

4. Generalized Simulation of Predicted Ionospheric Densities During an SEP Event

[23] The methods used in the preceding sections of this paper to predict ionospheric densities are time-consuming.

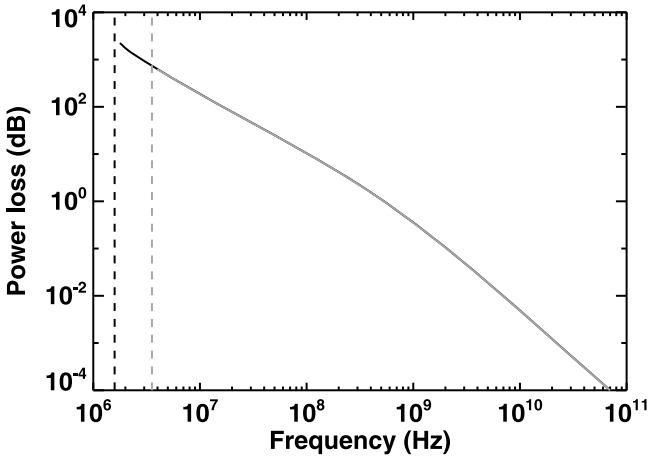

Figure 11. Power loss as function of radio wave frequency (solid lines) predicted from focused simulation of the 29 September 1989 SEP event. The black solid line corresponds to ionization by solar energetic particles only, neglecting photoionization, and the grey solid line corresponds to ionization by solar energetic particles and subsolar photoionization. The black and grey vertical dashed lines mark the frequencies at which a radio wave cannot propagate through the ionospheric plasma due to the maximum plasma frequency in the ionosphere exceeding the frequency of the radio wave.

They are not suitable for time-dependent case studies of selected events, which are required for the detailed interpretation of observations of actual SEP events at Mars. We label the results of this section as those of the "generalized simulation".

[24] The three main observable consequences of changes to the ionosphere during an SEP event are modifications to the vertical profile of electron density, total electron content, and radio wave absorption. The 70–100 km region of the ionosphere is critical for at least two of these observables. First (section 3.1), the most likely region for a radio occultation observation to easily and convincingly reveal changes in the electron density profile is 70–100 km, where electron densities are predicted to be significantly larger than their normal barely detectable values. Second (section 3.3), the 70–100 km region is where substantial contributions to radio wave absorption occur, since attenuation is most effective at high neutral densities yet electron densities drop considerably below 70 km due to the importance of water group ions. Third (section 3.2), and least critical, for our focused simulation of the ionization caused by solar energetic particles (neglecting photoionization), this region has a column-integrated electron content 10^{11} cm^{-2}, or about 30% of the total electron content of 3.5×10^{11} cm^{-2}. Therefore we strive for a simplified representation of ionospheric conditions during an SEP event that is accurate in the 70–100 km region. We use a neutral atmosphere derived from that of *Haider et al.* [2009] in which the number density of carbon dioxide is 2.35×10^{12} cm^{-3} at 100 km and varies exponentially with altitude with a scale height of 8.12 km. This is shown in Figure 3 as the idealized atmosphere.

4.1. Generalized Energy Deposition Profile

[25] Ionospheric conditions in the 70–100 km region are predominantly controlled by energetic particles whose stopping altitude lies in this region or just below. Thus 1–10 MeV particles are most important here (Figure 2b). The energy spectrum can be simplified, as indicated in Figure 1 by a dashed line, by neglecting the knee at high energies that is represented in equation (2) by the $\exp(-E/E_0)$ term. The range, R, that a proton of a particular initial energy travels before coming to rest is also well-approximated for energies of 1–500 MeV as:

$$R = \beta\left(E/E_{ref}\right)^{s} \tag{4}$$

where $\beta = 2.5 \times 10^{-3}$ g cm^{-2}, $E_{ref} = 1$ MeV and $s = 1.76$. This is indicated in Figure 2a by a dashed line. These simplifications can be substituted into equation (2). The stopping altitude z_S, which is significant in equation (2), satisfies $\int_{z'=z_S}^{z=\infty} \rho(z')dz' = R$ or $\rho(z_S)H = R$, where H is the neutral scale height and $\rho(z_S)H$ is the column density above z_S. Using equation (4), the density ρ_S at the stopping altitude for energy E satisfies $E = E_{ref}(\rho_S H/\beta)^{1/s}$. Accordingly, equation (2) becomes:

$$\begin{aligned} QdzdE &= 2\pi k E_{ref}\left(\frac{E}{E_{ref}}\right)^{1-\gamma-s}\frac{\rho dz}{\beta}dE \text{ if } E > E_{ref}(\rho H/\beta)^{1/s} \\ QdzdE &= 0 \text{ if } E < E_{ref}(\rho H/\beta)^{1/s} \end{aligned} \tag{5}$$

[26] The energy deposition rate (MeV cm^{-3} s^{-1}), Ψ, is:

$$\begin{aligned} \Psi &= \int_{E=0}^{E=\infty} QdE = \int_{E=E_{ref}(\rho H/\beta)^{1/s}}^{E=\infty} QdE \\ \Psi &= \int_{E=E_{ref}(\rho H/\beta)^{1/s}}^{E=\infty} 2\pi k E_{ref}\left(\frac{E}{E_{ref}}\right)^{1-\gamma-s}\frac{\rho}{\beta}dE \\ \Psi &= \frac{2\pi k E_{ref}^2}{H}\left(\frac{1}{\gamma+s-2}\right)\left[\frac{\rho H}{\beta}\right]^{\frac{2-\gamma}{s}} \end{aligned} \tag{6}$$

[27] The slope of the incident energy spectrum is important — Ψ decreases with increasing altitude if $\gamma < 2$, but increases with increasing altitude if $\gamma > 2$, and is uniform if $\gamma = 2$. However, it is clear that infinitely large values of Ψ at high altitude are unphysical. In reality, this is prevented from occurring by the incident energy spectrum and range ceasing to follow the functional dependencies outlined in equations (1) and (4) to extremely low energies. With those caveats in mind, this generalized prediction of the energy deposition rate profile is shown on Figure 4a by a dashed line. The agreement is good considering the simplifications made. Discrepancies above 100 km can be traced to errors in the simplified range at energies below 1 MeV. Discrepancies below 20 km can be traced to the simplified energy spectrum's neglect of the high energy knee. Conveniently, results are highly accurate in the critical 70–100 km region.

4.2. Generalized Ionospheric Density Profile

[28] If the energy necessary to produce one ion-electron pair is t and the ion chemistry is dominated by the dissociative recombination of O_2^+ [*Martinis et al.*, 2003; *Fox and*

Yeager, 2006], then the principle of photochemical equilibrium requires that the electron density N satisfies [*Schunk and Nagy*, 2000]:

$$N^2 = \frac{\Psi}{t\alpha} = \frac{2\pi k E_{ref}^2}{t\alpha H}\left(\frac{1}{\gamma + s - 2}\right)\left[\frac{\rho H}{\beta}\right]^{\frac{2-\gamma}{s}} \quad (7)$$

where α is the dissociative recombination coefficient for O_2^+, which equals 3×10^{-7} cm^3 s^{-1} on Mars [*Schunk and Nagy*, 2000; *Martinis et al.*, 2003]. Note that a photochemical ionization rate, I_{PC}, can also be included if desired, leading to $\alpha N^2 = I_{PC} + \Psi/t$. However, if we concentrate solely on ion production by solar energetic particles, and use t = 35 eV (section 2.3) and the idealized atmosphere of pure carbon dioxide shown in Figure 3 and described earlier in section 4, then the resultant electron density profile is that shown by the dashed line in Figure 9. The agreement is good in the critical 70–100 km region, but weaker elsewhere. Discrepancies above 100 km can again be traced to errors in the simplified range at energies below 1 MeV. Discrepancies below 70 km can be traced to the failure of the assumption of dominance by O_2^+ (Figure 5).

[29] The predicted electron density and several other derived quantities such as total electron content and power loss are proportional to $\sqrt{k}$ (equation (7)). If $\gamma < 2$, then the predicted electron density increases with decreasing altitude. If $\gamma = 2$, then the predicted electron density is independent of altitude and satisfies equation (8). If $\gamma > 2$, then the predicted electron density decreases with decreasing altitude. The predicted electron density at fixed altitude decreases with increasing γ for physically plausible ranges of γ.

$$N^2 = \frac{2\pi k E_{ref}^2}{t\alpha H s} \quad (8)$$

4.3. Applications

[30] Equation (7) can be used to predict ionospheric conditions in the critical 70–100 km region at any stage of any SEP event given an incident energy spectrum and the neutral atmospheric profile. Results are grossly inaccurate below 70 km, where water group ions dominate, but only mildly inaccurate above 100 km. Can we be confident that 70 km is always the altitude at which water groups ions become dominant? If the height of this boundary moves up and down a lot, then predictions based on the 70–100 km results from this generalized model will be poor. A definitive answer awaits focused simulations for all possible incident energy spectra and neutral atmospheric profiles. However, the focused simulations of this work, *Haider et al.* [2009], and *Molina-Cuberos et al.* [2002] have all found 70 km to be the critical altitude, so it is reasonable to accept as a working hypothesis that 70 km as the upper boundary of dominance by water group ions. Generalized simulations based on this approach are highly suited for studies of how the ionosphere varies during an SEP event and for studies of a broad range of different SEP events, when a focused simulation of the ionospheric chemistry for each instance would place excessive demands on available computational resources.

[31] We now use this approach to calculate several aspects of the ionospheric response to generic SEP events as a function of SEP event parameters k, intensity, and γ, spectral slope. These findings can be used to support the interpretation of comparisons between observed SEP and ionospheric conditions and to estimate when the effects of a particular SEP event may have been detectable by a particular instrument. As previously noted, we use carbon dioxide abundances where the number density is 2.35×10^{12} cm^{-3} at 100 km and varies with a scale height of 8.12 km, and $\beta = 2.5 \times 10^{-3}$ g cm^{-2}, E_{ref} = 1 MeV, s = 1.76, $\alpha = 3 \times 10^{-7}$ cm^3 s^{-1}, and t = 35 eV. We consider k from 10^1 to 10^5 cm^{-2} s^{-1} sr^{-1} MeV^{-1}) and γ from 1 to 4. For transparency, we neglect photoionization so that the only ionization source is solar energetic particles.

[32] Figure 12 shows the generalized simulation's electron density at 80 km altitude as a function of k and γ. A reference altitude of 80 km was selected as being below the main photochemical ionospheric layers, but above the critical altitude of 70 km at which equation (7) fails. Figure 12 illustrates that even an energetic particle spectrum one hundred times less intense than the spectrum used here for focused simulation of the 29 September 1989 event produces electron densities in excess of 3000 cm^{-3} at 80 km. For instance, the electron density at 80 km equals 5000 cm^{-3} when $\gamma = 2$ and $k = 60$ cm^{-2} s^{-1} sr^{-1} MeV^{-1}. The predicted electron density is proportional to $\sqrt{k}$, as expected from equation (7). Its dependence in γ is relatively weak.

[33] Figure 13 shows the generalized simulation's TEC as a function of k and γ. Electron densities below 70 km (section 4.2) and above 200 km (section 4.1) were neglected in this calculation of TEC. TEC values are proportional to $\sqrt{k}$ (equation (7)) and depend more strongly on γ than does the electron density at 80 km. For context, the subsolar TEC due to photoionization is on the order of 8×10^{11} cm^2 [*Mendillo et al.*, 2004].

[34] Figure 14 shows the power loss at 5 MHz as a function of k and γ. Electron densities below 70 km (section 4.2) and above 200 km (section 4.1) were neglected in this calculation of power loss. Again, the power loss is proportional to $\sqrt{k}$ and, as for the electron density at 80 km, relatively insensitive to γ. More than 13 dB of attenuation occurs at 5 MHz for $k > 30$ cm^{-2} s^{-1} sr^{-1} MeV^{-1}. This is an estimate for the threshold intensity at which an SEP event produces detectable MARSIS blackouts. Coincidentally, a very similar SEP intensity is required to produce electron densities at 80 km that exceed the measurement uncertainty of current radio occultation investigations, which is about 3×10^3 cm^{-3} [*Withers*, 2010, and references therein].

[35] This threshold intensity ($k > 30$ cm^{-2} s^{-1} sr^{-1} MeV^{-1}, about one percent of the 29 September 1989 event) corresponds to a significant SEP event. For comparison to historical records of SEP events, a different threshold is useful because k is not commonly used to report SEP event intensities. An alternative metric is the proton flux at energies greater than 10 MeV, which is used by NOAA to compare solar proton events that affected the terrestrial environment (http://umbra.gsfc.nasa.gov/SEP/). This flux is often reported in "proton flux units" or pfu, where 1 pfu = 1 proton cm^{-2} s^{-1} sr^{-1} at energies above 10 MeV. A "severe energetic particle event" is designated as one exceeding 10 pfu. Our 29 September 1989 event reached 4500 pfu at Earth. An inverse-square extrapolation to Mars orbit at

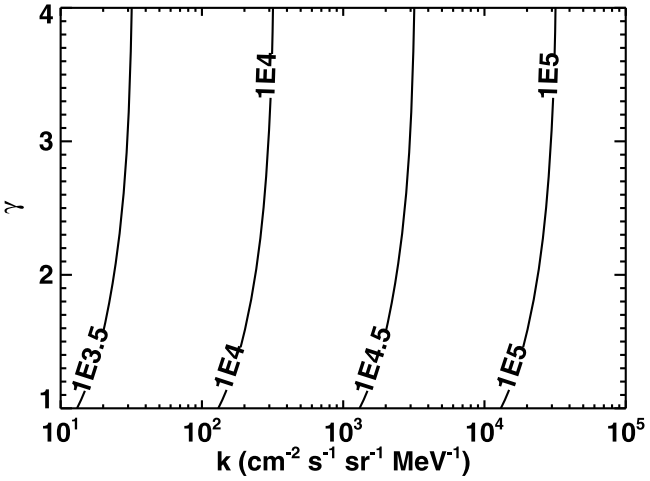

Figure 12. Electron density (units of cm^{-3}) at 80 km predicted for a general SEP event by the generalized approach of section 4 as a function of SEP event parameters k, intensity, and γ, spectral slope.

1.5 AU predicts an intensity of 2000 pfu at Mars), so a value 100 times smaller than this (45 pfu at Earth, 20 pfu at Mars) can be considered as the threshold at which we predict SEP events have detectable effects at Mars. The occurrence rate of such events varies from zero per year in deep solar minima to around ten per year at solar maximum. *Morgan et al.* [2006, Figure 2] reports several blackout periods during July–September 2005. The two longest-lasting correspond to the Bastille Day storm (14–15 July, 134 pfu at Earth, 60 pfu at Mars) and the 8–11 September event (1880 pfu at Earth, 840 pfu at Mars). Another blackout is associated with the 22–23 August event (330 pfu at Earth, 147 pfu at Mars). Two moderate blackout periods around 3 August and 27 August do not correspond to events listed at http://umbra.gsfc.nasa.gov/SEP/ and the event of 27–29 July

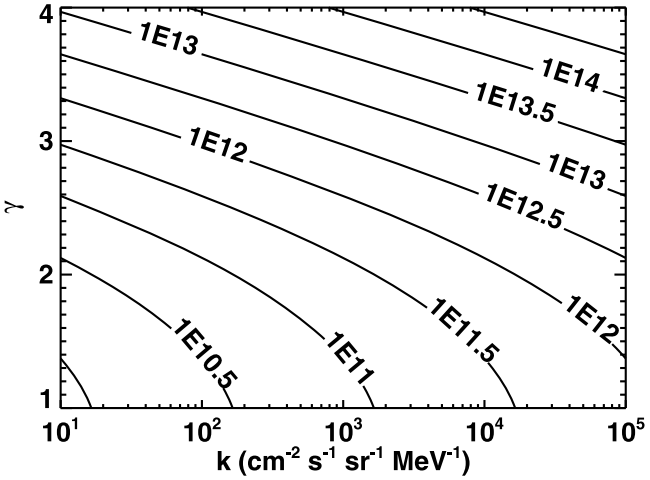

Figure 13. Total electron content (TEC) between 70 km and 200 km (units of cm^{-2}) predicted for a general SEP event by the generalized approach of section 4 as a function of SEP event parameters k, intensity, and γ, spectral slope.

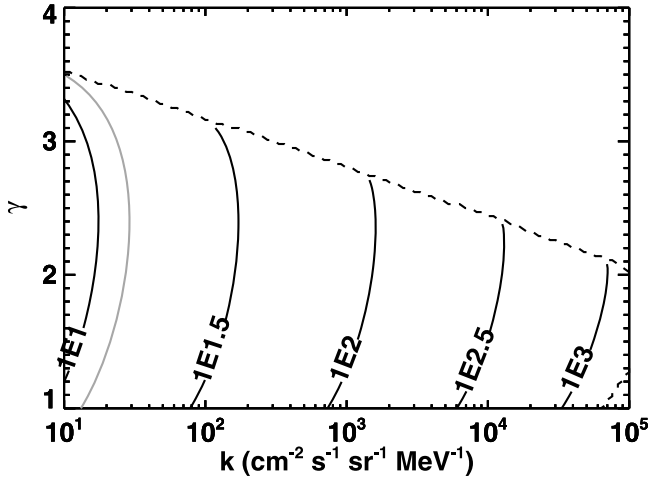

Figure 14. Power loss (dB) predicted at 5 MHz for a general SEP event by the generalized approach of section 4 as a function of SEP event parameters k, intensity, and γ, spectral slope. Calculations are based on electron densities between 70 km and 200 km. The grey solid contour indicates the 13 dB ($13 = 10^{1.11}$) of power loss required for a MARSIS blackout. The dashed black line marks regions where a 5 MHz radio wave cannot propagate through the ionospheric plasma due to the maximum plasma frequency in the ionosphere (70–200 km) exceeding the frequency of the radio wave.

(41 pfu at Earth, 18 pfu at Mars) did not cause a MARSIS blackout. Our predicted threshold intensity is consistent with the observations of *Morgan et al.* [2006].

5. Summary and Conclusions

[36] We have used simulations of the energy deposition rate during a large SEP event to predict how ionospheric densities are increased by the event. A straight-forward representation of energy deposition was used, which may result in predicted ionospheric densities being overestimated, but by a factor of no more than three. If only ion production by energetic particles is considered, thereby neglecting photoionization, then electron densities during the 29 September 1989 SEP event exceeded 10^4 cm^{-3} from 30 km to 130 km. Such large electron densities are rare below about 100 km altitude. The large vertical extent of this region of dense ionospheric plasma is in stark contrast to the narrower effects of other disturbances that can enhance plasma densities below 100 km, namely solar flares and meteoroids. According to these predictions, the ionospheric response to a large SEP event should be clearly visible in any radio occultation measurements acquired at such a time. However, a survey of radio occultation measurements did not find such strong responses. The predicted increase in TEC, about 50% of the subsolar TEC, is also significant and should be detectable by orbiting radar instruments. This effect was detected by *Lillis et al.* [2010]. It is unclear why the predicted enhancement in TEC is observed when the predicted enhancement in electron densities near 100 km is not. The predicted radio wave attenuation at 5 MHz at the peak of this SEP event is tremendous, 1000 dB, and more than sufficient to mask MARSIS surface reflections. These

simulations support the hypothesis that SEP events cause these MARSIS blackouts. The predicted radio wave attenuation is also large at higher frequencies and may be detectable in other data sets.

[37] We have also derived an analytical expression for the electron density profile during an SEP event that is valid above about 70 km, where O_2^+ ions, not water group ions, dominate the ionospheric chemistry. It assumes an energy spectrum characterized by a single power law, in contrast to one that turns over at high energies, and a dependence of range on energy that is also characterized by a single power law. Despite these assumptions being valid in only a limited altitude range, the analytical expression leads to useful results. This is because this region is precisely where the most significant impact of SEP events on observable electron density, total electron content, and radar attenuation occurs. This analytical expression can be used to qualitatively determine the magnitude and duration of the impact of selected SEP events on the Martian environment. It is also useful for highlighting the key physical processes associated with the ionospheric response to an SEP event, as well as the relationships between them and the resultant state of the ionosphere, and has the potential for ready application to other solar system ionospheres.

[38] **Acknowledgments.** P.W. acknowledges Hermann Opgenoorth and an anonymous colleague for helpful reviews, productive discussions with members of the Living With a Star Targeted Research and Technology "Extreme space weather events in the solar system" Focus Team led by Yingjuan Ma, comments from Dave Brain, a survey of MGS electron densities by Zachary Girazian, and partial support from NASA grant NNX08AP96G.

[39] Philippa Browning thanks the reviewers for their assistance in evaluating this paper.

References

Agren, K., et al. (2007), On magnetospheric electron impact ionisation and dynamics in Titan's ram-side and polar ionosphere–A Cassini case study, *Ann. Geophys.*, *25*, 2359–2369, doi:10.5194/angeo-25-2359-2007.

Bailey, D. K. (1964), Polar-cap absorption, *Planet. Space Sci.*, *12*, 495–541, doi:10.1016/0032-0633(64)90040-6.

Basu, B., J. R. Jasperse, D. J. Strickland, and R. E. Daniell Jr. (1993), Transport-theoretic model for the electron-proton-hydrogen atom aurora: 1. Theory, *J. Geophys. Res.*, *98*, 21,517–21,532, doi:10.1029/93JA01646.

Berger, M. J., J. S. Coursey, M. A. Zucker, and J. Chang (2005), ESTAR, PSTAR, and ASTAR: Computer Programs for Calculating Stopping-Power and Range Tables for Electrons, Protons, and Helium Ions (version 1.2.3), http://physics.nist.gov/star, Natl. Instit. of Stand. and Technol., Gaithersburg, Md.

Bisikalo, D. V., V. I. Shematovich, J.-C. Gérard, G. R. Gladstone, and J. H. Waite (1996), The distribution of hot hydrogen atoms produced by electron and proton precipitation in the Jovian aurora, *J. Geophys. Res.*, *101*, 21,157–21,168, doi:10.1029/96JE01952.

Budden, K. G. (1985), *The Propagation of Radio Waves*, Cambridge Univ. Press, Cambridge, U. K.

Capone, L. A., R. C. Whitten, J. Dubach, S. S. Prasad, and W. T. Huntress Jr. (1976), The lower ionosphere of Titan, *Icarus*, *28*, 367–378, doi:10.1016/0019-1035(76)90150-0.

Deghfel, B., M. Nekkab, and A. Kahoul (2009), M X-ray production cross sections for heavy elements by proton impact, *X Ray Spectrom.*, *38*, 399–405, doi:10.1002/xrs.1191.

Desorgher, L., E. O. Flückiger, M. Gurtner, M. R. Moser, and R. Bütikofer (2005), Atmocosmics: A Geant 4 code for computing the interaction of cosmic rays with the Earth's atmosphere, *Int. J. Mod. Phys. A*, *20*, 6802–6804, doi:10.1142/S0217751X05030132.

Fox, J. L., and A. Dalgarno (1979), Ionization, luminosity, and heating of the upper atmosphere of Mars, *J. Geophys. Res.*, *84*, 7315–7333, doi:10.1029/JA084iA12p07315.

Fox, J. L., and K. E. Yeager (2006), Morphology of the near-terminator martian ionosphere: A comparison of models and data, *J. Geophys. Res.*, *111*, A10309, doi:10.1029/2006JA011697.

Fox, J. L., M. I. Galand, and R. E. Johnson (2008), Energy deposition in planetary atmospheres by charged particles and solar photons, *Space Sci. Rev.*, *139*, 3–62, doi:10.1007/s11214-008-9403-7.

Gaisser, T. K. (1990), *Cosmic Rays and Particle Physics*, Cambridge Univ. Press, Cambridge, U. K.

Galand, M., and S. Chakrabarti (2002), Auroral processes in the solar system, in *Atmospheres in the Solar System: Comparative Aeronomy*, *Geophys. Monogr. Ser.*, vol. 130, edited by M. Mendillo, A. Nagy, and J. H. Waite, pp. 55–76, AGU, Washington, D. C.

Galand, M., J. Lilensten, W. Kofman, and R. B. Sidje (1997), Proton transport model in the ionosphere: 1. Multistream approach of the transport equations, *J. Geophys. Res.*, *102*, 22,261–22,272, doi:10.1029/97JA01903.

Gronoff, G., J. Lilensten, L. Desorgher, and E. Flückiger (2009), Ionization processes in the atmosphere of Titan I Ionization in the whole atmosphere, *Astron. Astrophys.*, *506*, 955–964, doi:10.1051/0004-6361/200912371.

Gronoff, G., C. Mertens, J. Lilensten, L. Desorgher, E. Flückiger, and P. Velinov (2011), Ionization processes in the atmosphere of Titan. III. Ionization by high-Z nuclei cosmic rays, *Astron. Astrophys.*, *529*, A143, doi:10.1051/0004-6361/201015675.

Haider, S. A., M. A. Abdu, I. S. Batista, J. H. Sobral, X. Luan, E. Kallio, W. C. Maguire, M. I. Verigin, and V. Singh (2009), D, E, and F layers in the daytime at high-latitude terminator ionosphere of Mars: Comparison with Earth's ionosphere using COSMIC data, *J. Geophys. Res.*, *114*, A03311, doi:10.1029/2008JA013709.

Hinson, D. P., R. A. Simpson, J. D. Twicken, G. L. Tyler, and F. M. Flasar (1999), Initial results from radio occultation measurements with Mars Global Surveyor, *J. Geophys. Res.*, *104*, 26,997–27,012.

International Commission on Radiation Units and Measurements (1993), *Average Energy Required to Produce an Ion Pair*, Int. Comm. on Radiat. Units and Meas.), Washington, D. C.

Jokipii, J. R., C. P. Sonett, and M. S. Giampapa (1997), *Cosmic Winds and the Heliosphere*, Univ. of Arizona Press, Tucson.

Kallio, E., and S. Barabash (2001), Atmospheric effects of precipitating energetic hydrogen atoms on the Martian atmosphere, *J. Geophys. Res.*, *106*, 165–178, doi:10.1029/2000JA002003.

Lario, D., A. Aran, and R. B. Decker (2009), Major solar energetic particle events of solar cycles 22 and 23: Intensities close to the streaming limit, *Sol. Phys.*, *260*, 407–421, doi:10.1007/s11207-009-9463-1.

Leblanc, F., J. G. Luhmann, R. E. Johnson, and E. Chassefiere (2002), Some expected impacts of a solar energetic particle event at Mars, *J. Geophys. Res.*, *107*(A5), 1058, doi:10.1029/2001JA900178.

Lillis, R. J., D. A. Brain, S. L. England, P. Withers, M. O. Fillingim, and A. Safaeinili (2010), Total electron content in the Mars ionosphere: Temporal studies and dependence on solar EUV flux, *J. Geophys. Res.*, *115*, A11314, doi:10.1029/2010JA015698.

Lovell, J. L., M. L. Duldig, and J. E. Humble (1998), An extended analysis of the September 1989 cosmic ray ground level enhancement, *J. Geophys. Res.*, *103*, 23,733–23,742, doi:10.1029/98JA02100.

Luhmann, J. G., and J. U. Kozyra (1991), Dayside pickup oxygen ion precipitation at Venus and Mars: Spatial distributions, energy deposition and consequences, *J. Geophys. Res.*, *96*, 5457–5467, doi:10.1029/90JA01753.

Martinis, C. R., J. K. Wilson, and M. J. Mendillo (2003), Modeling day-to-day ionospheric variability on Mars, *J. Geophys. Res.*, *108*(A10), 1383, doi:10.1029/2003JA009973.

Mendillo, M., X. Pi, S. Smith, C. Martinis, J. Wilson, and D. Hinson (2004), Ionospheric effects upon a satellite navigation system at Mars, *Radio Sci.*, *39*, RS2028, doi:10.1029/2003RS002933.

Mendillo, M., P. Withers, D. Hinson, H. Rishbeth, and B. Reinisch (2006), Effects of solar flares on the ionosphere of Mars, *Science*, *311*, 1135–1138, doi:10.1126/science.1122099.

Mertens, C. J., B. T. Kress, M. Wiltberger, S. R. Blattnig, T. S. Slaba, S. C. Solomon, and M. Engel (2010), Geomagnetic influence on aircraft radiation exposure during a solar energetic particle event in October 2003, *Space Weather*, *8*, S03006, doi:10.1029/2009SW000487.

Meyer-Vernet, N. (2007), *Basics of the Solar Wind*, Cambridge Univ. Press, Cambridge, U. K.

Molina-Cuberos, G. J., H. Lichtenegger, K. Schwingenschuh, J. J. López-Moreno, and R. Rodrigo (2002), Ion-neutral chemistry model of the lower ionosphere of Mars, *J. Geophys. Res.*, *107*(E5), 5027, doi:10.1029/2000JE001447.

Morgan, D. D., D. A. Gurnett, D. L. Kirchner, R. L. Huff, D. A. Brain, W. V. Boynton, M. H. Acuña, J. J. Plaut, and G. Picardi (2006), Solar control of radar wave absorption by the Martian ionosphere, *Geophys. Res. Lett.*, *33*, L13202, doi:10.1029/2006GL026637.

Nielsen, E., D. D. Morgan, D. L. Kirchner, J. Plaut, and G. Picardi (2007), Absorption and reflection of radio waves in the Martian ionosphere, *Planet. Space Sci.*, *55*, 864–870, doi:10.1016/j.pss.2006.10.005.

O'Brien, K. (1969), Extra-nuclear hadron cascade calculations using Passow's approximation, *Nucl. Instrum. Methods*, *72*, 93–98, doi:10.1016/0029–554X(69)90271–7.

Parkinson, C. D., D. A. Brain, M. W. Liemohn, R. J. Lillis, and S. W. Bougher (2010), Hot hydrogen/proton precipitation in planetary ionospheres, Abstract SM41B-1870 presented at 2010 Fall Meeting, AGU, San Francisco, Calif., 13–17 Dec.

Patterson, J. D., T. P. Armstrong, C. M. Laird, D. L. Detrick, and A. T. Weatherwax (2001), Correlation of solar energetic protons and polar cap absorption, *J. Geophys. Res.*, *106*, 149–164, doi:10.1029/2000JA002006.

Porter, H. S., and A. E. S. Green (1975), Comparison of Monte Carlo and continuous slowing-down approximation treatments of 1-keV proton energy deposition in N_2, *J. Appl. Phys.*, *46*, 5030–5038, doi:10.1063/1.321493.

Reames, D. V., C. K. Ng, and A. J. Tylka (2001), Heavy ion abundances and spectra and the large gradual solar energetic particle event of 2000 July 14, *Astrophys. J.*, *548*, L233–L236, doi:10.1086/319100.

Rees, M. H., and R. A. Jones (1973), Time dependent studies of the aurora —II. Spectroscopic morphology, *Planet. Space Sci.*, *21*, 1213–1235, doi:10.1016/0032–0633(73)90207–9.

Schrijver, C. J., and G. L. Siscoe (2010), *Heliophysics*, Cambridge Univ. Press, Cambridge, U. K.

Schunk, R. W., and A. F. Nagy (2000), *Ionospheres*, Cambridge Univ. Press, New York.

Simon, C., J. Lilensten, J. Moen, J. M. Holmes, Y. Ogawa, K. Oksavik, and W. F. Denig (2007), TRANS4: A new coupled electron/proton transport code–comparison to observations above Svalbard using ESR, DMSP and optical measurements, *Ann. Geophys.*, *25*, 661–673, doi:10.5194/angeo-25-661-2007.

Withers, P. (2009), A review of observed variability in the dayside ionosphere of Mars, *Adv. Space Res.*, *44*, 277–307, doi:10.1016/j.asr.2009.04.027.

Withers, P. (2010), Prediction of uncertainties in atmospheric properties measured by radio occultation experiments, *Adv. Space Res.*, *46*, 58–73, doi:10.1016/j.asr.2010.03.004.

Withers, P. (2011), Attenuation of radio signals by the ionosphere of Mars: Theoretical development and application to MARSIS observations, *Radio Sci.*, *46*, RS2004, doi:10.1029/2010RS004450.

Withers, P., M. Mendillo, D. P. Hinson, and K. Cahoy (2008), Physical characteristics and occurrence rates of meteoric plasma layers detected in the martian ionosphere by the Mars Global Surveyor Radio Science Experiment, *J. Geophys. Res.*, *113*, A12314, doi:10.1029/2008JA013636.